

Periodicity-induced effects in the scattering and absorption of light by infinite and finite gratings of circular silver nanowires

Denys M. Natarov,^{1,*} Volodymyr O. Byelobrov,¹ Ronan Sauleau,²
Trevor M. Benson,³ and Alexander I. Nosich¹

¹Laboratory of Micro and Nano-Optics, Institute of Radio-Physics and Electronics NASU, Kharkiv 61085, Ukraine

²George Green Institute for Electromagnetics Research, University of Nottingham, NG7 2RD, Nottingham, UK

³Institut d'Electronique et Telecommunications de Rennes, Universite de Rennes 1, Rennes 35042, France

*den.natarov@gmail.com

Abstract: We study numerically the effect of periodicity on the plasmon-assisted scattering and absorption of visible light by infinite and finite gratings of circular silver nanowires. The infinite grating is a convenient object of analysis because of the possibility to reduce the scattering problem to one period. We use the well-established method of partial separation of variables however make an important improvement by casting the resulting matrix equation to the Fredholm second-kind type, which guarantees convergence. If the silver wires have sub-wavelength radii, then two types of resonances co-exist and may lead to enhanced reflection and absorption: the plasmon-type and the grating-type. Each type is caused by different complex poles of the field function. The low-Q plasmon poles cluster near the wavelength where dielectric function equals -1 . The grating-type poles make multiplets located in close proximity of Rayleigh wavelengths, tending to them if the wires get thinner. They have high Q-factors and, if excited, display intensive near-field patterns. A similar interplay between the two types of resonances takes place for finite gratings of silver wires, the sharpness of the grating-type peak getting greater for longer gratings. By tuning carefully the grating period, one can bring together two resonances and enhance the resonant scattering of light per wire by several times.

©2011 Optical Society of America

OCIS codes: (050.0050) Diffraction and gratings; (050.1970) Diffractive optics; (290.0290) Scattering.

References and links

1. For example, examination of the single-cylinder field Fourier expansion coefficients (177) of [7] for $ka = 2\pi a / \lambda \rightarrow 0$ shows that they have poles at $\lambda = \lambda_n^P$, for which $\varepsilon(\lambda_n^P) \approx -1 - c_n (ka)^2 (4n)^{-1}$, where the azimuthal index is $n \geq 1$ and $c_n > 0$ are known coefficients.
2. J. Kottmann, O. Martin, D. Smith, and S. Schultz, "Plasmon resonances of silver nanowires with a nonregular cross-section," *Phys. Rev. B* **64**(23), 235402 (2001).
3. J. Kottmann and O. J. F. Martin, "Plasmon resonant coupling in metallic nanowires," *Opt. Express* **8**(12), 655–663 (2001).
4. V. Giannini and J. A. Sánchez-Gil, "Calculations of light scattering from isolated and interacting metallic nanowires of arbitrary cross section by means of Green's theorem surface integral equations in parametric form," *J. Opt. Soc. Am. A* **24**(9), 2822–2830 (2007).
5. T. Søndergaard and S. J. Bozhevolnyi, "Strip and gap plasmon polariton optical resonators," *Phys. Status Solidi B* **245**(1), 9–19 (2008).
6. F. J. G. García de Abajo, "Colloquium: Light scattering by particle and hole arrays," *Rev. Mod. Phys.* **79**(4), 1267–1290 (2007).
7. V. Twersky, "On scattering of waves by the infinite grating of circular cylinders," *IRE Trans. Antennas Propag.* **10**(6), 737–765 (1962).
8. O. Kavaklioglu, "On diffraction of waves by the infinite grating of circular dielectric cylinders at oblique incidence: Floquet representation," *J. Mod. Phys.* **48**, 125–142 (2001).

9. K. Yasumoto, H. Toyama, and T. Kushta, "Accurate analysis of 2-D electromagnetic scattering from multilayered periodic arrays of circular cylinders using lattice sums technique," *IEEE Trans. Antenn. Propag.* **52**(10), 2603–2611 (2004).
10. R. Gómez-Medina, M. Laroche, and J. J. Sáenz, "Extraordinary optical reflection from sub-wavelength cylinder arrays," *Opt. Express* **14**(9), 3730–3737 (2006).
11. M. Laroche, S. Albaladejo, R. Gomez-Medina, and J. J. Saenz, "Tuning the optical response of nanocylinder arrays: an analytical study," *Phys. Rev. B* **74**(24), 245422 (2006).
12. M. Laroche, S. Albaladejo, R. Carminati, and J. J. Sáenz, "Optical resonances in one-dimensional dielectric nanorod arrays: field-induced fluorescence enhancement," *Opt. Lett.* **32**(18), 2762–2764 (2007).
13. V. O. Byelobrov, J. Ctyroky, T. M. Benson, R. Sauleau, A. Altintas, and A. I. Nosich, "Low-threshold lasing eigenmodes of an infinite periodic chain of quantum wires," *Opt. Lett.* **35**(21), 3634–3636 (2010).
14. L. Rayleigh, "On the dynamical theory of gratings," *Proc. R. Soc. Lond., A Contain. Pap. Math. Phys. Character* **79**(532), 399–416 (1907).
15. A. Hessel and A. A. Oliner, "A new theory of Wood's anomalies on optical gratings," *Appl. Opt.* **4**(10), 1275–1297 (1965).
16. D. W. Kerr and C. H. Palmer, "Anomalous behavior of thin-wire gratings," *J. Opt. Soc. Am.* **61**(4), 450–456 (1971).
17. S. Zou, N. Janel, and G. C. Schatz, "Silver nanoparticle array structures that produce remarkably narrow plasmon lineshapes," *J. Chem. Phys.* **120**(23), 10871–10875 (2004).
18. S. Zou and G. C. Schatz, "Narrow plasmonic/photonic extinction and scattering line shapes for one and two dimensional silver nanoparticle arrays," *J. Chem. Phys.* **121**(24), 12606–12612 (2004).
19. S. Zou and G. C. Schatz, "Silver nanoparticle array structures that produce giant enhancements in electromagnetic fields," *Chem. Phys. Lett.* **403**(1-3), 62–67 (2005).
20. E. M. Hicks, S. Zou, G. C. Schatz, K. G. Spears, R. P. Van Duyn, L. Gunnarsson, T. Rindzevicius, B. Kasemo, and M. Käll, "Controlling plasmon line shapes through diffractive coupling in linear arrays of cylindrical nanoparticles fabricated by electron beam lithography," *Nano Lett.* **5**(6), 1065–1070 (2005).
21. N. Félidj, G. Laurent, J. Aubard, G. Lévi, A. Hohenau, J. R. Krenn, and F. R. Aussenegg, "Grating-induced plasmon mode in gold nanoparticle arrays," *J. Chem. Phys.* **123**(22), 221103 (2005).
22. V. G. Kravets, F. Schedin, and A. N. Grigorenko, "Extremely narrow plasmon resonances based on diffraction coupling of localized plasmons in arrays of metallic nanoparticles," *Phys. Rev. Lett.* **101**(8), 087403 (2008).
23. B. Auguié and W. L. Barnes, "Collective resonances in gold nanoparticle arrays," *Phys. Rev. Lett.* **101**(14), 143902 (2008).
24. S. V. Boriskina and L. Dal Negro, "Multiple-wavelength plasmonic nanoantennas," *Opt. Lett.* **35**(4), 538–540 (2010).
25. V. Twersky, "On a multiple scattering theory of the finite grating and the Wood anomalies," *J. Appl. Phys.* **23**(10), 1099–1118 (1952).
26. G. O. Olaofe, "Scattering by two cylinders," *Radio Sci.* **5**(11), 1351–1360 (1970).
27. H. A. Ragheb and M. Hamid, "Scattering by N parallel conducting circular cylinders," *Int. J. Electron.* **59**(4), 407–421 (1985).
28. A. Z. Elsherbeni and A. A. Kishk, "Modeling of cylindrical objects by circular dielectric and conducting cylinders," *IEEE Trans. Antenn. Propag.* **40**(1), 96–99 (1992).
29. D. Felbacq, G. Tayeb, and D. Maystre, "Scattering by a random set of parallel cylinders," *J. Opt. Soc. Am. A* **11**(9), 2526–2538 (1994).
30. X. Antoine, C. Chniti, and K. Ramdani, "On the numerical approximation of high-frequency acoustic multiple scattering problems by circular cylinders," *J. Comput. Phys.* **227**(3), 1754–1771 (2008).
31. Here, we imply convergence in mathematical sense, as a possibility to minimise the error in the solution by inverting progressively greater matrices. Non-convergent numerical solutions are often able to provide a couple of correct digits however fail to achieve better accuracy.
32. X. Antoine, K. Ramdani, and B. Thierry, "Etude numerique de la resolution par equations integrales de la diffraction multiple par des disques," in *Proc. Congres Français d'Acoustique*, Lyon (2010).
33. P. B. Johnson and R. W. Christy, "Optical constants of the noble metals," *Phys. Rev.* **6**(12), 4370–4379 (1972).
34. A. I. Nosich, "Radiation conditions, limiting absorption principle, and general relations in open waveguide scattering," *J. Electromagn. Waves Appl.* **8**(3), 329–353 (1994).
35. C. M. Linton, "The Green's function for the two-dimensional Helmholtz equation in periodic domains," *J. Eng. Math.* **33**(4), 377–401 (1998).
36. V. Giannini, G. Vecchi, and J. Gómez Rivas, "Lighting up multipolar surface plasmon polaritons by collective resonances in arrays of nanoantennas," *Phys. Rev. Lett.* **105**(26), 266801 (2010).
37. R. F. Oulton, V. J. Sorger, T. Zentgraf, R.-M. Ma, C. Gladden, L. Dai, G. Bartal, and X. Zhang, "Plasmon lasers at deep subwavelength scale," *Nature* **461**(7264), 629–632 (2009).
38. W. Zhou and T. W. Odom, "Tunable subradiant lattice plasmons by out-of-plane dipolar interactions," *Nat. Nanotechnol.* **6**(7), 423–427 (2011).

1. Introduction

Localized surface plasmon resonances (P-resonances) and their applications in biosensors, nanoantennas and nanolasers are hot topics in today's photonics. Besides of the spherical and rod-like particles, metal nanowires are also attractive as elementary scatterers able to display

intensive P-resonances if illuminated with a light polarized orthogonally to the wire axis (so-called H-polarization case). If the length of a nanowire makes several or more free-space wavelengths, the scattering of light can be studied using a two-dimensional (2-D) model. This circumstance has led to extensive study of the P-assisted plane-wave scattering by stand-alone noble-metal wires of various shapes, from circular to strip-like rectangular to polygonal. For a circular wire, the separation of variables leads to analytical solution for the scattered field albeit in the form of an infinite series. For a sub-wavelength circular silver wire, this solution shows a single broad scattering peak slightly red-shifted from the wavelength $\lambda^p = 338$ nm [1,2] where the dielectric function of silver is $\text{Re}\varepsilon(\lambda^p) = -1$. A closer study shows that the peak is caused by the presence of an infinite number of closely spaced P-eigenmodes having azimuthal orders $n \neq 1$ [1]. The corresponding scattering resonances, however, merge together because at that wavelength the silver is lossy, $\text{Im}\varepsilon(\lambda^p) \approx 0.31$, although the resonant near field of a circular wire is dominated by the dipole terms with $n = \pm 1$. Non-circular wire analysis needs more elaborate techniques such as volume integral equations (IEs) [2,3] or boundary IEs [4,5]. They reveal not one but many shape and illumination-angle dependent P-resonances of different types and azimuthal orders. The same is valid for configurations built from two or three wires (2-D dimers and trimers) [3–6].

Thus, on the one hand, the scattering of light by a single and a pair of sub-wavelength circular noble-metal wires has been analyzed extensively and the associated P-resonances have been demonstrated and quantified. However larger ensembles of such wires, notably their periodically structured collections, remain less studied.

On the other hand, the scattering of plane waves by free-standing *infinite* periodic gratings of circular cylinders made of conventional dielectrics has also been extensively studied as a canonical scattering problem (see [7–9]). This includes the recently found existence of specific grating-type (G) resonances (a.k.a. “geometric” and “lattice” resonances) both in the E- and H-polarization cases [6,10–13]. For a grating of thin wires they appear just above the “Rayleigh passing-off wavelengths” (at the normal incidence, this is $\lambda_m^R = p/m$, $m = 0, \pm 1, \dots$ [14,15]) associated with branch points of the field as a function of the wavelength. Here, it is necessary to remember that the resonances of various types are associated with the complex poles of the field function [15]. The reason for overlooking G-resonances earlier can be seen in their extreme proximity to the branch-point Rayleigh wavelengths λ_m^R , especially for thin-wire gratings. This intrinsically implies that G-resonances have high Q-factors even in the presence of losses in the wire material. If the wires can be pumped to create inverse population (quantum wires), the same G-modes demonstrate ultra-low thresholds of lasing [13]. Still real-life grids of wires are finite; hence it is interesting to find out how the G-type resonances develop themselves in finite thin-wire gratings. The only previous study of this effect seems to be [16] however it had stopped short of the correct explanation.

Finally, if the material of sub-wavelength wires is a noble metal such as silver, then both P-type and G-type resonances may exist together in the visible range. Their explicit strengths should depend on the fine structure of the scatterer and appear to be not studied so far. Therefore in this paper we undertake such a study.

Here, it should be noted that several years ago it was found that finite periodic chains of nanosize noble-metal spheres may display enhanced scattering of light at the wavelength very close to the period value. This was at first predicted theoretically using the simple dipole approximation of each sphere [17] and then supported by simulations based on the Discrete Dipole Approximation and T-matrix methods [18,19]. Later, narrow resonances with half-width of just several nanometers were directly observed in regular arrays of metallic nanoparticles near Rayleigh’s cutoff wavelengths in [20–23]. Their nature has been at first linked exclusively to the plasmons, therefore early-days terminology included “radiatively non-decaying plasmons,” “supernarrow plasmon resonances,” and “plasmon resonances based on diffraction coupling of localized plasmons.” More close to the point was the “collective resonance” term of [23]. Recently it was proposed to build multifrequency nano-antennas

from finite arrays of particles [24] whose periods are tuned to the sensing wavelengths to achieve a “photonic resonance.” However from what is said above, it is quite clear that [17–24] dealt, in fact, with the G-resonances and not with plasmons, although the latter resonances were also present. Thus, our study of the 2-D scattering by the silver wire gratings may shed light on the nature of the 3-D scattering by gratings of metal particles.

Our method of analysis is not completely new. Its foundation can be traced to the works of V. Twersky and others in the 1950s on the scattering by infinite gratings and finite collections of circular cylinders [25–30]. It is based on the Fourier expansions of the field in the local polar coordinates and the use of addition theorems for cylindrical functions (in the 3-D scattering by spherical particles a similar method is called the generalized Mie theory). However, we have noticed one very important defect of earlier papers. Namely, they used such a form of the final matrix equations (for instance, (11) and (206) of [7]) that were good for extracting low-frequency or thin-wire asymptotic solutions but which did not provide the convergence if one builds a numerical solution [31]. This means that on replacing the infinite-order equation with its counterpart that is truncated to the order N , one cannot approach the accurate solution by taking N progressively larger. Examples of numerical catastrophe at $N \rightarrow \infty$ can be seen in [30]. We have found, however, that this defect can be removed by re-scaling the unknown coefficients. This yields an algorithm that is able to deliver results that are accurate to machine precision. All numerical results in our paper are based on such correct algorithm. The proper scaling of unknowns appears automatically if one works with equivalent electric and magnetic currents on the surface of wires – this was done in [32].

In the modeling of the plasmon-assisted scattering, one has to account accurately for the dispersion of the complex dielectric function of silver $\varepsilon(\lambda)$. A frequent approach is to use the Drude formula with specific values of the constants needed to fit the measured wavelength dependence. However, it is known that the Drude model fails to achieve good fits of both $\text{Re}\varepsilon(\lambda)$ and $\text{Im}\varepsilon(\lambda)$; the choice is usually done in favor of $\text{Re}\varepsilon(\lambda)$ and then the losses are characterized inaccurately. Therefore we use the experimental data for the both parts taken from [33] and arrange an Akima spline interpolation between the experimental values.

In our work, we restrict ourselves to numerical study of the H-polarization only, although G-resonances on silver-wire gratings exist in the E-case as well, unlike P-resonances. Because of the lack of space, we present only the results for the normal incidence of a plane wave. This is because at an inclined incidence, the scattering behavior becomes quite messy as Rayleigh wavelengths λ_m^R and λ_{-m}^R become different and each of them is accompanied with a multiplet of G-resonances similar to those studied here. By the same reason we do not present here a study of the near-field enhancement and will address this topic in a separate publication. Still the resonance effects found here have their obvious manifestations in the field enhancement as well simply because of the presence of corresponding poles of the field function.

In the remainder of the paper, we start from the analysis of scattering by an infinite periodic grating of silver wires because it can be reduced to a single period (Section 2). After that we study the scattering and absorption of light by finite gratings of such wires (Section 3). A comparison of infinite and finite gratings is briefly discussed in Section 4. The results of our work are then presented in Summary.

2. Infinite grating scattering

Consider a grating made of circular cylinders in free space, placed parallel to the z -axis and periodic along the x -axis – see Fig. 1. Denote the grating period as p , the wire radius as a , and the refractive index as ν . We suppose that the field is time-harmonic $\sim \exp(-i\omega t)$ and does not vary along the z -axis. Then two alternative polarizations can be considered using a function U that is either the E_z or the H_z field component, respectively.

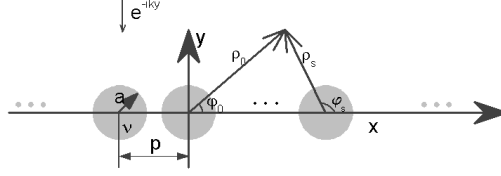


Fig. 1. Infinite periodic grating of circular cylinders illuminated by a normally incident plane wave.

This function must satisfy the Helmholtz equation with appropriate wavenumber inside and outside of cylinders, the Sveshnikov radiation condition [34] at infinity, the condition of local integrability of power, and the boundary conditions demanding continuity of the tangential field components at the cylinder boundary. The free-space wavenumber is $k = \omega / c = 2\pi / \lambda$, where c is the light velocity and λ is the wavelength, while inside the cylinders it is kv .

Consider the normal incidence of a plane wave, $U^0(x, y) = e^{-iky}$. Then, according to the Floquet theorem, the scattered field is a periodic function of x with period p . In this case we can study the field within one elementary cell of the grating, say $|x| \leq p/2$. Here, the circular shape of the wire cross-section suggests that the secondary field can be expanded in terms of the azimuth angle in the polar coordinates co-axial with the wire,

$$U^{int}(x, y) = \sum_{n=-\infty}^{\infty} a_n J_n(kvr) e^{in\varphi}, \quad r < a, \quad (1)$$

$$U^{ext}(x, y) = U^0 + \sum_{n=-\infty}^{\infty} b_n \left[H_n(kr) e^{in\varphi} + \sum_{l=-\infty}^{\infty} S_{n-l}(kp) J_l(kr) e^{il\varphi} \right], \quad r > a, \quad (2)$$

$$S_{2q}(kp) = 2 \sum_{s=1}^{\infty} H_{2q}(skp), \quad S_{2q+1}(kp) = 0, \quad (3)$$

where J_m and H_m are the Bessel and the Hankel first-kind functions, respectively.

Performing mathematical operations similar to [7–9] we derive an infinite matrix equation for the field expansion coefficients b_n . However, unlike [7–9] we emphasize that this equation has to be cast in the so-called Fredholm second kind form. This is achieved by re-scaling the unknown coefficients as $b_n = x_n J_n(ka)$, so that we obtain

$$X + AX = B, \quad X = \{x_m\}_{m=-\infty}^{+\infty}, \quad A = \{A_{mn}\}_{m,n=-\infty}^{+\infty}, \quad B = \{B_m\}_{m=-\infty}^{+\infty}, \quad (4)$$

$$A_{mn} = \frac{S_{n-m}(2\pi\sigma) V_m(u, v) J_n(u)}{F_m(u, v) J_m(u)}, \quad B_m = \frac{(-1)^m V_m(u, v)}{F_m(u, v) J_m(u)}, \quad (5)$$

$$F_m^{E,H} = \beta^{E,H} H_m(u) J_m'(vu) - H_m'(u) J_m(vu), \quad V_m^{E,H} = \beta^{E,H} J_m(u) J_m'(vu) - J_m'(u) J_m(vu), \quad (6)$$

where we have denoted $u = ka = 2\pi\sigma / \xi$, $\sigma = p / \lambda = ka\xi / 2\pi$, $\xi = p / a$, $\beta^{E,H} = v^{\pm 1}$, and the prime denotes differentiation in argument. Note that the *lattice sums* can be cast to [7]

$$S_0(2\pi\sigma) = -1 - \frac{2i}{\pi} [\gamma + \log(\sigma / 2)] + \frac{1}{\pi\sigma} + \frac{2}{\pi} \sum_{s=1}^{\infty} \left[\frac{1}{(\sigma^2 - s^2)^{1/2}} + \frac{i}{s} \right], \quad (7)$$

$$S_{2q}(2\pi\sigma) = \frac{2}{\pi} \sum_{s=1}^{\infty} \frac{e^{-2iq\theta_s}}{(\sigma^2 - s^2)^{1/2}} + \frac{1}{\pi\sigma} + \frac{i}{q\pi} + \frac{i}{\pi} \sum_{s=1}^q \frac{(-1)^s (q+s-1)! 2^{2s}}{(2s)!(q-s)! \sigma^{2s}} D_{2s}, \quad q = 1, 2, \dots \quad (8)$$

where γ is Euler's constant, $\theta_s = \arcsin(s/\sigma)$, and D_{2s} are Bernoulli's numbers.

The rescaling applied above provides $\sum_{n,m=-\infty}^{+\infty} |A_{nm}|^2 < \infty$ and $\sum_{m=-\infty}^{+\infty} |B_m|^2 < \infty$, if only $p > 2a$ (i.e. if cylinders do not touch each other). This is a crucially important property because it guarantees the convergence of solutions of the truncated equation to exact one if the order N of truncation gets greater [31]. In the numerical results presented below, $N = 3$ to 5 guaranteed four correct digits in the near field computations and comparison with [9] revealed two-digit agreement. Note that denser gratings need larger N to obtain the same accuracy.

One can see from Eqs. (7) and (8) that $S_q(2\pi\sigma)$ have both branch points and poles at $\lambda = \lambda_s^R$. They converge very slowly and therefore, acceleration procedures are necessary - see details in [35]. Outside of the grating domain (the strip of the width $2a$), the scattered field can be conveniently converted to the series in terms of the Floquet spatial harmonics,

$$U^{ext,\pm}(x,y) = \sum_{s=-\infty}^{\infty} f_s^{\pm} e^{ik\pi_s x} e^{ik\tau_s |y|}, \quad f_s^{\pm} = (\pi\sigma\tau_s)^{-1} \sum_{n=-\infty}^{\infty} x_n J_n(ka)(-i\pi_s \pm \tau_s)^n, \quad (9)$$

where $\pi_s = s/\sigma$, $\tau_s = (1 - \pi_s^2)^{1/2}$, $\text{Re } \tau_s \geq 0$ or $\text{Im } \tau_s \geq 0$. Then the power fractions reflected and transmitted by the grating (per one period) are the reflectance and transmittance,

$$R_{inf} = \sum_{\gamma_s < k} |f_s^+|^2, \quad T_{inf} = |1 + f_0^-|^2 + \sum_{\gamma_s < k, s \neq 0} |f_s^-|^2, \quad (10)$$

and power conservation implies that $R_{inf} + T_{inf} + A_{inf} = 1$ where A_{inf} is the absorbance.

Any dielectric wire grating is a periodic open resonator. It possesses a discrete set of complex-valued natural frequencies σ coinciding with the roots of determinantal equation, $\text{Det}[I + A(\sigma, \xi, \nu)] = 0$. The Fredholm nature of Eq. (4), together with Gerschgorin theorem, ensures that these eigenvalues lie in finite circles centered at the zeros of the diagonal elements, i.e. the roots of $1 + A_{mm}(\sigma, \xi, \nu) = 0$. This property immediately reveals three types of natural frequencies: (i) those tending to zeros of $F_m(ka, \nu)$ with finite νka if $\sigma \rightarrow \infty$; they generate the quasi-eigenmodes of a stand-alone wire perturbed by other wires, (ii) those tending to zeros of $\nu^2(k) + 1$ if both $\sigma \rightarrow \infty$ and $\nu ka \rightarrow 0$; they generate the plasmon quasi-eigenmodes of a single wire perturbed by other wires, and (iii) those tending to the poles of $S_0(2\pi\sigma)$ if $(\nu - 1)ka \rightarrow 0$; they generate the grating quasi-eigenmodes caused by periodicity.

After separation of Eq. (4) into two independent equations for the symmetric and anti-symmetric across the x -axis parts, the eigenfrequencies of the corresponding x -symmetric G-eigenmodes are found in the form of asymptotic expressions valid for $\delta = \pi^4 \xi^{-4} \rightarrow 0$,

$$\sigma_{m,0}^{GH+} = m - im^5(m\pi - 1)^{-1}(\nu^2 - 1)\delta - (1/2m^{1/2})m^8(\nu^2 - 1)^2\delta^2, \quad (11)$$

$$\sigma_{m,n}^{GH+} = m - \frac{im^{4n+1}(\nu^2 - 1)(\nu^2 + 1)^{-1}\delta^n}{2^{2n+1}(2n)!(2n-1)!(m\pi - 2)} - \frac{8m^{8n}(\nu^2 - 1)^2(\nu^2 + 1)^{-2}\delta^{2n}}{4^{2n}[(2n)!(2n-1)!]^2}, \quad n = 1, 2, \dots, \quad (12)$$

Thus, if the wire radius gets smaller, both for lossless and lossy materials, the Q-factors of the G-modes grow up as $O(\xi^4)$ and their frequencies tend to Rayleigh's frequencies at least as $O(\xi^{-4})$. The same happens if the contrast between the wire and host medium vanishes.

It should be emphasized that G-resonances (i.e. corresponding poles of the field function) are present in the scattering by the gratings of both conventional-dielectric wires, PEC wires, and noble-metal wires. This is unlike P-resonances existing only for noble-metal wires [1–6]. Today the non-plasmon nature of G-resonances seems to be clearly realized by only some researchers (e.g., [23,24]); others still consider them as specific plasmons as certified by the

titles of papers [20–22]. In part, this is probably caused by the fact that when both P and G-resonances exist together, the combined-resonance spectral responses can produce a wide variety of complicated Fano shapes [23], depending on the wavelengths and linewidths or real and imaginary parts of corresponding P and G-poles on the complex-wavelength plane.

Consider now the numerical results for the H-polarized plane wave normally incident on the infinite periodic grating of circular wires made of silver, in the visible range of wavelengths.

In Fig. 2, we present reliefs of the reflectance R_{inf} and absorbance $A_{\text{inf}} = 1 - T_{\text{inf}} - R_{\text{inf}}$ of the infinite grating as a function of two variables: the wavelength within the visible band and the wire radius, for periods $p = 450$ nm and 350 nm. Note also that the plots of spectral dependences of these values for fixed a and p can be seen in the last figure of this paper.

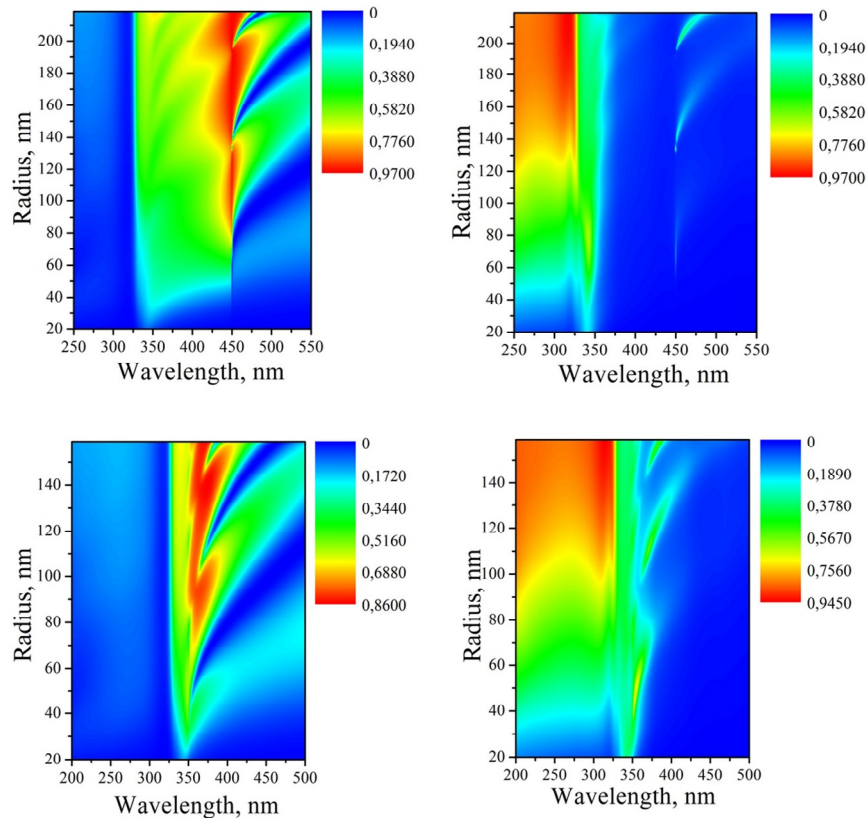


Fig. 2. Reflectance (left panels) and absorbance (right panels) of infinite grating of silver wires as a function of the wavelength and wire radius for the normal incidence of the H-polarized plane wave. The period is $p = 450$ nm for the upper panels and $p = 350$ nm for the lower ones.

As mentioned, a stand-alone sub-wavelength silver wire displays a broad peak of scattering, slightly red-shifted from $\lambda = 338$ nm [1,2], usually called P-resonance. If an infinite grating is sparse ($p - 2a < a$, or $a/p < 0.3$), then the optical coupling between the wires is weak and a “ridge” corresponding to the P-resonance peak is found at the same wavelength. For denser gratings (with fixed period, this means for thicker wires; in Fig. 2 this is for $a > 150$ nm), one can see that several weaker peaks spin off to the red side, being associated with higher P-multipoles due to increased optical coupling between the adjacent wires. Besides of the broad P-resonance, one can see a sharper ridge of increased reflection

and absorption at a wavelength close to, however slightly larger than, the period. This is the G-resonance [10–13] caused by the presence of the multiplet of G-poles, $GH_{l,n}^{\pm}$, which become well separated for wires of larger radii ($a > 150$ nm) due to stronger optical coupling. Note that if $a \rightarrow 0$ then the width of the G-type resonance shrinks as explained above [Eq. (11)]; this resonance takes a Fano shape with a maximum followed by a sharp minimum, not resolved for $a < 75$ nm.

In Fig. 3, we show reliefs of reflectance and absorbance versus the wavelength and the period for fixed $a = 70$ nm where G-resonance lies just above the line $\lambda = p$. It becomes stronger coming to the P-resonance that appears as a broader ridge at $330 \text{ nm} < \lambda < 350 \text{ nm}$.

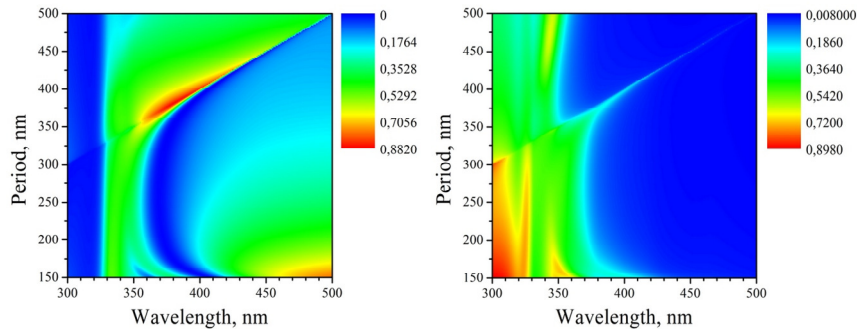


Fig. 3. Reflectance (left) and absorbance (right) of the infinite grating of silver wires as function of the wavelength and period for the normal incidence of the H-polarized plane wave. Wires' radii are $a = 70$ nm.

It is interesting to visualize the in-resonance field patterns because in the vicinity of the grating they are dominated by the corresponding quasi-eigenmode patterns. In Fig. 4, we present the total near fields in the P (a) and G resonances (b), corresponding to the grating of the upper panels in Fig. 2, and in the combined resonance (c) corresponding to lower panels. One can see certain common features of the patterns in well-separated P and G-resonances: shadows in the lower half-space and standing waves caused by the intensive reflection in the upper half-space. However in the P-resonance the field hot spots are seen at the illuminated (upper) faces of each wire, and above the grating the field is a superposition of the 0-th and the ± 1 -st Floquet spatial harmonics. In the cases of the isolated G-type resonance and the mixed P-G resonance (Figs. 4 (b,c)) the grating vicinity is dominated by the very intensive standing wave, $U(x, y) \approx 2f_1^{\pm} e^{ik\tau_1|y|} \cos(k\pi x) = \text{const} \cdot Q e^{-k|y|/Q} \cos(2\pi x/p) + O(1)$. It is built from two resonating ± 1 -st Floquet harmonics whose amplitudes $|f_1^{\pm}| \approx O(Q) \gg 1$ are not restricted by the power conservation law because they decay along the y -axis as $\tau_1^2 < 0$.

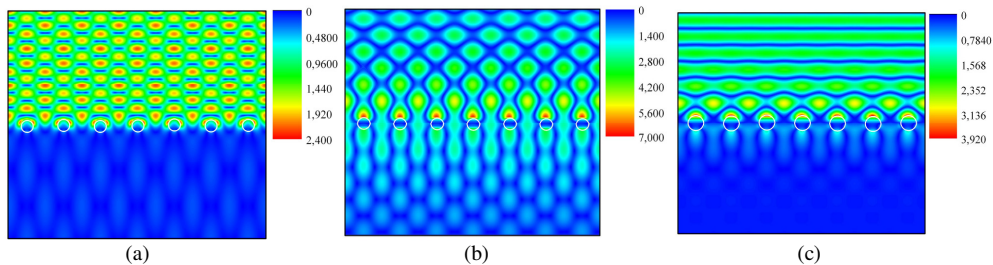


Fig. 4. Near-field patterns: (a) in the P-resonance ($\lambda = 340.8$ nm) and (b) in the G-resonance ($\lambda = 451.35$ nm) for the grating of silver wires with radii $a = 90$ nm and period $p = 450$ nm, and (c) in the combined P-G resonance for the grating of $a = 90$ nm and $p = 350$ nm ($\lambda = 362.45$ nm). See Figs. 2 and 3 for the corresponding values of reflectance and absorbance of these gratings. A plane wave is incident from the upper half-space.

3. Finite grating scattering

Consider now a finite grating of M identical circular wires with radii a and refractive index ν located along the x -axis with period p and illuminated by the plane H-polarised wave incident at angle φ_0 (see Fig. 5).

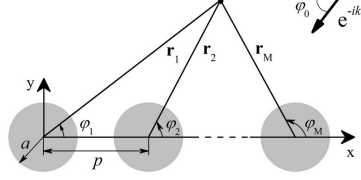


Fig. 5. Finite periodic grating of circular cylinders illuminated by a plane wave.

This 2-D scattering problem can be treated along the same lines as for the infinite grating, with the radiation condition changed to more conventional Sommerfeld condition. Now, however, one cannot use the Floquet theorem and reduce consideration to single period. On expanding the field function in terms of the azimuth exponents in the local coordinates (r_q, φ_q) , $q = 1, \dots, M$, using addition theorems for cylindrical functions, applying the boundary conditions on the surface of all cylinders, and re-scaling the coefficients as explained above, we obtain an $M \times M$ block-type matrix equation where each block is infinite,

$$X + \tilde{A}X = \tilde{B}, \quad X = \{X^{(q)}\}_{q=1}^M, \quad X^{(q)} = \{x_m^{(q)}\}_{m=-\infty}^{+\infty}, \quad (13)$$

$$\tilde{A} = \{\tilde{A}^{(q,j)}\}_{q,j=1}^M, \quad \tilde{A}^{(q,j)} = \{\tilde{A}_{m,n}^{(q,j)}\}_{m,n=-\infty}^{+\infty}, \quad \tilde{B} = \{\tilde{B}^{(q)}\}_{q=1}^M, \quad \tilde{B}^{(q)} = \{\tilde{B}_m^{(q)}\}_{m=-\infty}^{+\infty}, \quad (14)$$

$$\tilde{A}_{m,n}^{(q,j)} = \frac{H_l(l|q-j|2\pi\sigma)V_m(u,\nu)J_n(u)}{F_m(u,\nu)J_m(u)}, \quad \tilde{B}_m^{(q)} = \frac{(-i)^m V_m(u,\nu)}{F_m(u,\nu)J_m(u)} e^{-i2\pi\sigma(q-1)\cos\varphi_0 + im\varphi_0}, \quad (15)$$

where $l = \text{sign}(q-j) \times (m-n)$, $u = ka$, and $\sigma = p/\lambda$.

For a finite chain of wires, we cannot compute the reflectance as we did for the infinite grating. Instead, we will compute the total scattering cross-section (TSCS) found as

$$S_{sc} = \frac{2}{\pi k} \int_0^{2\pi} |\Phi(\varphi)|^2 d\varphi, \quad \Phi(\varphi) = \sum_{n=-\infty}^{+\infty} (-i)^n J_n(u) \left[\sum_{q=1}^M x_n^{(q)} e^{-i2\pi\sigma(q-1)\cos\varphi} \right] e^{in\varphi}. \quad (16)$$

Note that the sum of TSCS and absorption cross-section (ACS) is the extinction cross-section; it is linked to the magnitude of the scatterer shadow by the optical theorem,

$$S_{sc} + S_{ab} = -(4/k) \text{Re} \Phi(\varphi_0 + \pi), \quad (17)$$

We emphasize that unlike [25–30], if $p > 2a$ then Eq. (13) is a Fredholm second kind matrix equation, because $\sum_{n,m=-\infty}^{+\infty} |A_{mn}^{(i,j)}|^2 < \infty$, $(i, j = 1, \dots, M)$. Thanks to this fact, the sequence of solutions of counterpart equations with each block truncated to finite order N converges to exact solution if $N \rightarrow \infty$. As a test, we have compared our code against the numerical data of [2,3,26–28] and found full graphical agreement.

In Figs. 6 to 9, we present some results concerning the scattering and absorption of the H-polarized plane waves by finite gratings of sub-wavelength silver nanowires. They have been computed with $N = 3$ to 5; this provided 4 correct digits in the near-field characteristics.

The most interesting question is what the peak values of the grating characteristics become if the P and the G-resonance wavelengths coincide. Here, the main instrument of tuning them together is the period of the wire grating, because P-resonance has almost fixed wavelength

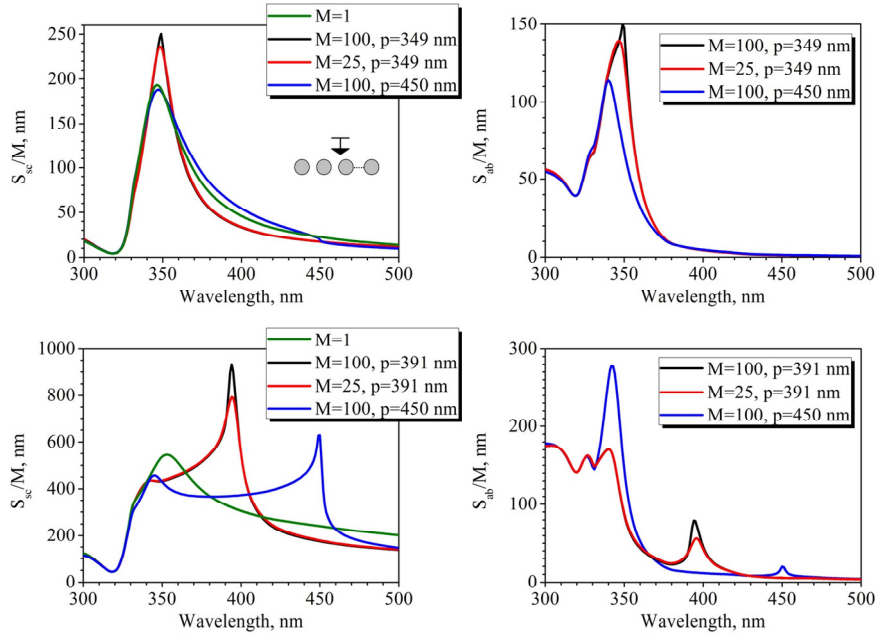


Fig. 6. TSCS (left panels) and ACS (right panels) per silver wire versus the wavelength for the normal incidence ($\varphi_0 = \pi/2$) at the gratings of $M = 100$ wires with radii $a = 30$ nm (upper panels) and 70 nm (lower panels).

near to the single-wire value, λ^P . For instance, the spectra of TSCS and ACS for a stand-alone silver nanowire with radius of 30 and 70 nm have broad maxima at 348 nm and 349 nm, respectively. In Fig. 6, similar plots of TSCS and ACS per silver wire are presented for several sparse gratings of $M = 100$ wires of the same values of radius. One can see that the G-resonance for the gratings with period having values far from the P-resonance wavelength λ^P has almost no effect on TSCS: the former is only a small spike standing on the broad shoulder of the latter. This behavior changes drastically, however, if the G-resonance is tuned nearer to λ^P : in that case there appears a much more intensive resonance. For a grating of $M = 100$ wires of $a = 70$ nm, the peak value of TSCS per wire is 1.7 times higher than for a stand-alone wire with the same radius and is red-shifted by 42 nm to $\lambda = 391$ nm. As we have found, the optimal values of the wire radius to observe the strongest TSCS enhancement lie in the range of 25 nm to 70 nm.

More complete information on the behavior of TSCS and ACS normalized by M is presented in Figs. 7 and 8. Here we show reliefs of the mentioned quantities as functions of the wavelength and the radius and period, respectively, for the gratings of $M = 100$ silver wires. In the upper panels of Fig. 7, the P and G-resonances are well separated standing near to λ^P and $\lambda_1^R = p$, respectively, and G-resonance shows higher-order sub-resonances spinning off to the red for thicker wires. In the lower panels, two resonances overlap.

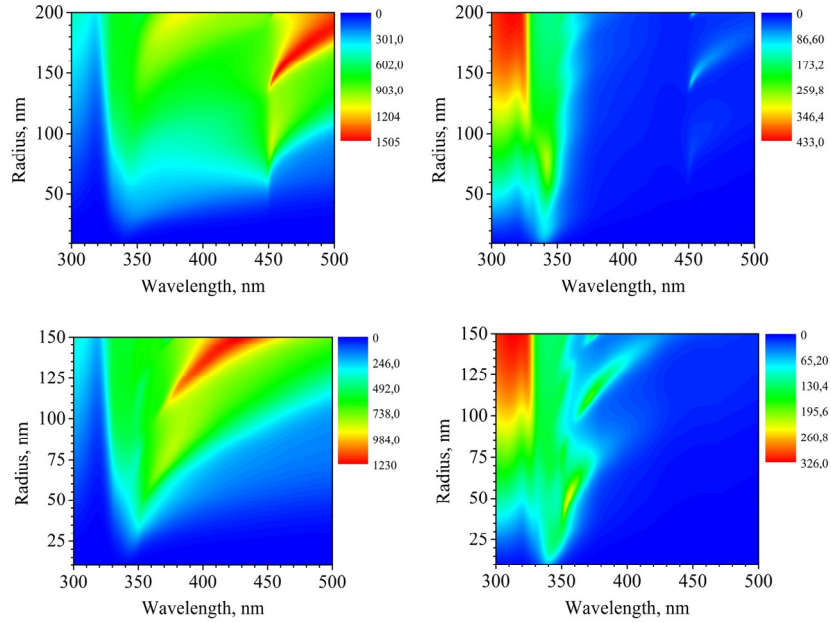


Fig. 7. Per-wire TSCS (left panels) and ACS (right panels) versus the wavelength and the period for linear gratings of $M = 100$ silver nanowires with period $p = 450$ nm (upper panels) and 350 nm (lower panels).

In Fig. 8, clearly visible bright “ridges” of enhanced scattering and absorption stretch just above the line $\lambda = p$ and approach it for larger periods. For finite gratings, this line does not correspond to a branch point and the “ridges” are caused by the G-poles only. In contrast, P-resonances are visible as vertical (less bright) “ridges” around the 345 nm wavelength for sparse gratings. Maximum scattering occurs at the crossing of two “ridges.” For dense gratings ($p < 200$ nm), the P-resonance red-shifts because of the stronger optical coupling.

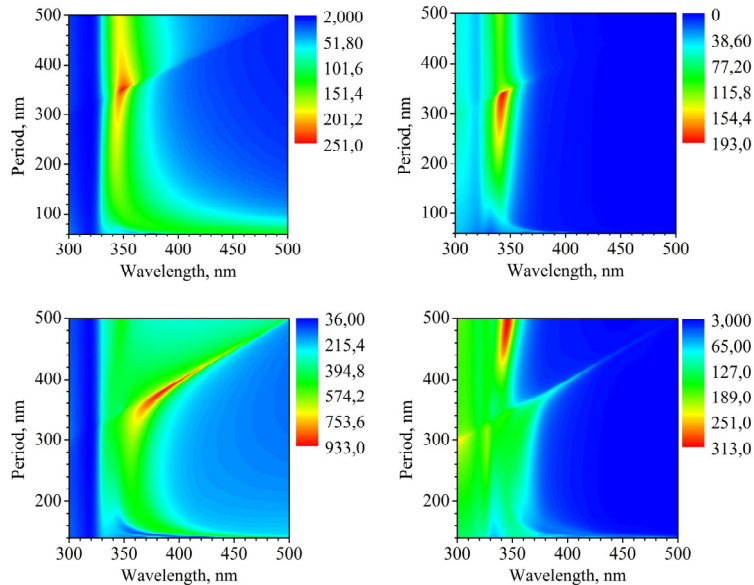


Fig. 8. Per-one wire TSCS (left panels) and ACS (right panels) versus the wavelength and the period for the gratings of $M = 100$ silver nanowires with radii $a = 30$ nm (upper panels) and 70 nm (lower panels).

Figure 9 (a),(b), presents the near-field amplitude and phase patterns for a 25-wire sparse grating with $a = 30$ nm and $p = 349$ nm in the combined P-G resonance at 348 nm. For comparison, in Fig. 9 (c),(d) we show similar near-field patterns in the combined P-G resonance on the 25-wire sparse grating with $a = 70$ nm and $p = 391$ nm at the wavelength of 394 nm. The wires are shown as white circles.

In both cases the field hot-spot maxima are visible near the illuminated sides of the wires similarly to the single-wire case [2,4]. In addition to these hot spots, one can clearly see two intensive local standing waves: one is above the grating, formed by the incident plane wave and the reflected field. Another standing wave is especially visible in the lower panels. This is an “orthogonal” wave standing along the grating and stretching to the distance of 2-3 periods above the cylinders. This standing wave has bright maxima of opposite phase near the wires and between them (see also Fig. 4 and associated discussion), as it is formed by two oppositely propagating ± 1 -st quasi-Floquet harmonics. Such a near field pattern is a signature of the G-resonance.

We believe that these results are potentially important for understanding and interpreting the electromagnetic properties of novel efficient periodically structured optical nano-antennas [24,36], nano-lasers [13,37], and plasmon-assisted biosensor substrates [38].

4. How large is infinity?

It is interesting to compare the scattering by infinite and finite gratings. However it is far from obvious how to select a proper figure-of-merit. We have found that the efficiency of a finite chain of wires of *reflecting* a plane wave can be introduced as the part of TSCS associated with the power scattered into the upper half-space and normalized by the wire diameter $2a$ and the number of wires M ,

$$\tilde{R}_{fin} = 1 / (\pi Mka) \int_0^\pi |\Phi(\varphi)|^2 d\varphi. \quad (18)$$

This quantity can be conveniently compared to the reflectance of an infinite grating (see Eq. (10)) normalized by the relative width subtended by a single wire, i.e. to $\tilde{R}_{inf} = \xi R_{inf} / 2$ ($\xi = p / a$). Fig. 10 presents such a comparison for gratings of circular silver nanowires having radii $a = 70$ nm and different periods from 350 to 490 nm.

As one can see, 10 wires of this radius are enough to provide normalized reflective efficiency within 10% of the infinite grating value in the whole band of wavelengths from 300 to 500 nm, except of the narrow band around the G-resonance where from 100 to probably 500 wires are needed to achieve the same effect. Still even gratings as short as 10 sub-wavelength silver wires display smoothed G-resonances with Fano-type behavior around the Rayleigh wavelength. The optimum grating period that provides the maximum value of reflective efficiency of 2.5 has been found to be $p = 391$ nm.

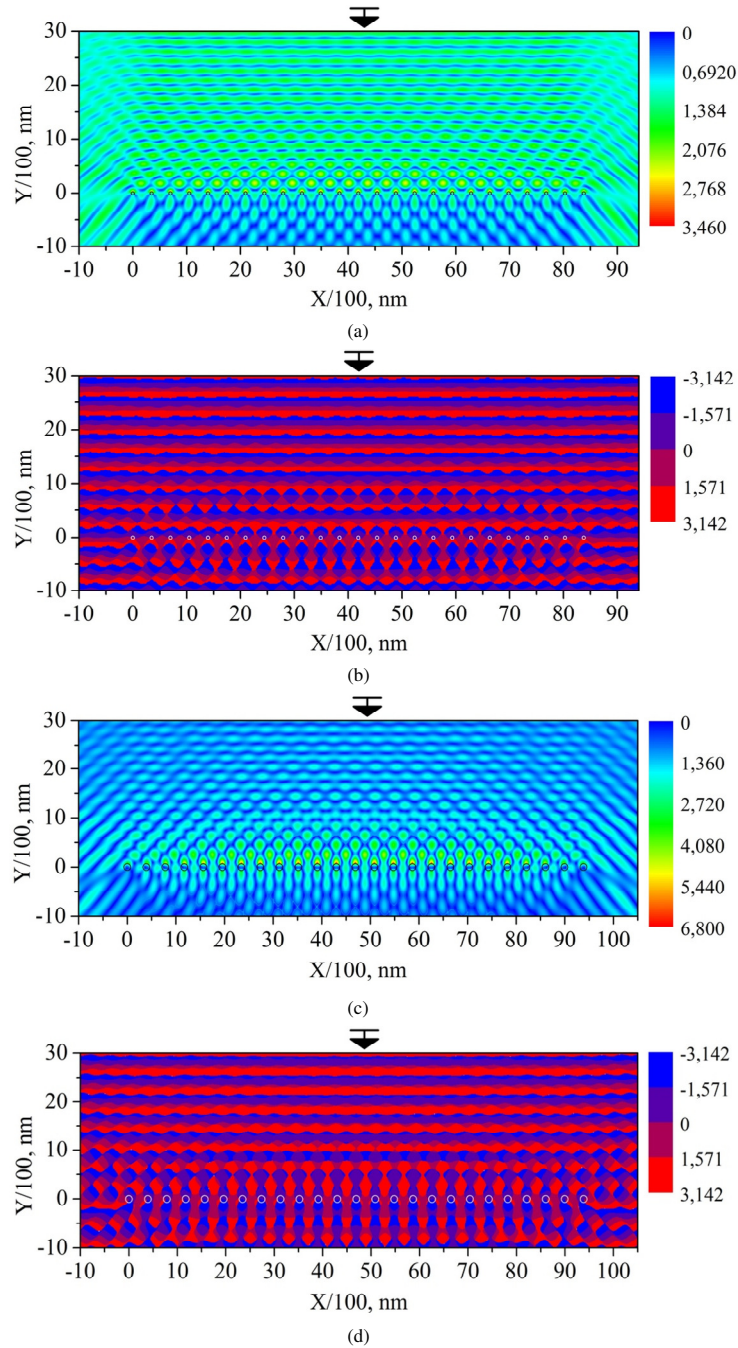


Fig. 9. Near-field amplitude (a, c) and phase (b, d) patterns in two combined P-G resonances for the H-wave normally incident ($\varphi_0 = \pi/2$) at the grating of $M = 25$ silver nanowires with $a = 30$ nm, $p = 349$ nm, at the wavelength 348 nm (a, b) and with $a = 70$ nm, $p = 391$ nm, at the wavelength $\lambda = 394$ nm (c, d).

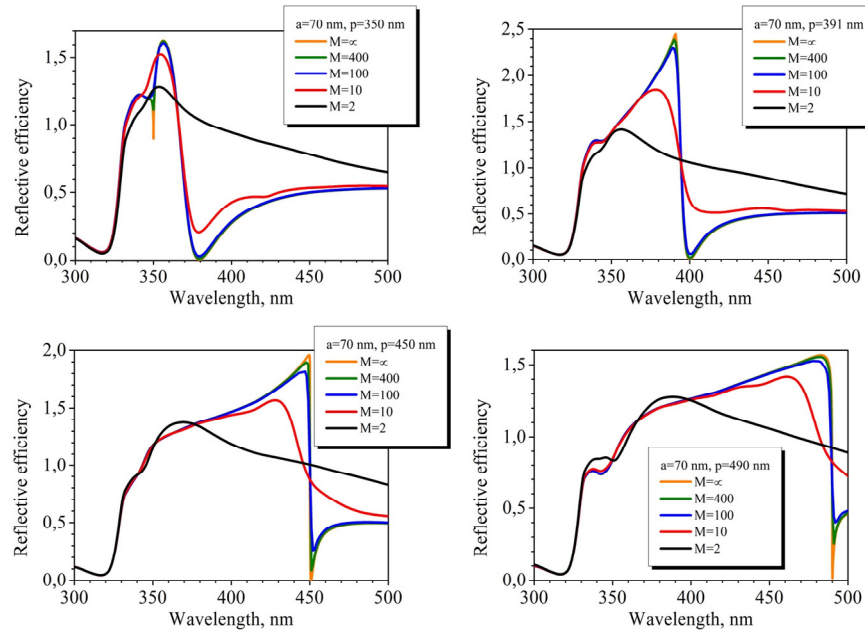


Fig. 10. Normalized reflective efficiency \tilde{R} as function of wavelength for finite and infinite gratings of silver nanowires with the radii of 70 nm and different periods. An H-polarized plane wave is at normal incidence.

5. Summary

Summarizing, we have presented mathematically grounded and numerically accurate to the fourth digit results for the scattering and absorption of an H-polarized plane wave by infinite and finite linear gratings of circular silver nanowires. This was achieved by using not a FDTD simulation but a classical multiple-scattering technique with accurate boundary and radiation conditions, corrected with respect to earlier papers to provide mathematical convergence. Using this accurate computational instrument, we have studied two types of resonances: plasmon and grating-type, and computed the configurations where these resonances are both well-separated and tuned together.

Plasmon resonance appears as a broad peak in the reflectance, reflective efficiency, or total scattering cross-section, slightly red-shifted from the wavelength where the real part of the dielectric function of silver equals to -1 . It has low Quality factor determined by the losses in silver. Grating resonances are very different as caused by the different complex poles of the field as a function of the wavelength. For infinite gratings, the well-separated grating resonances usually lead to total reflection, which is followed by zero reflection (a Fano shape). The exact shape of the combined P-G resonance strongly depends on the separation in wavelength between two resonances (i.e. between the real parts of their complex natural frequencies). For instance, if two resonances are brought together then G-resonance appears as a narrow minimum on the top of the broad P-resonance.

For a finite grating of sparsely located wires, the dynamics of the behavior of the scattering characteristics is quite similar. The peak value of TSCS per silver wire in the combined resonance can be several times greater in comparison to a single wire. The radius of wire optimal for enhanced scattering is between 25 and 70 nm, and the sharpness of the combined resonance peak depends on the number of wires. Another interesting observation is a characteristic standing wave in the case of the grating resonance or combined P-G resonance, i.e. at $\lambda = p + O(\xi^{-4})$. This wave stands along the grating as $\cos(2\pi x/p)$, has bright spots at the wires and in the middle between them, and dominates in the near field at the

illuminated side of grating. Such a near field pattern can be considered as a signature of the grating resonance.

Acknowledgments

This work was supported, in part, by the National Academy of Sciences of Ukraine via the State Target Program “Nanomaterials and Nanotechnologies” and the European Science Foundation via the Research Networking Programme “Newfocus.”